ELSEVIER

Nuclear Physics B 621 (2002) 3–34

NUCLEAR PHYSICS B

www.elsevier.com/locate/npe

A study of strange particle production in ν_μ charged current interactions in the NOMAD experiment

NOMAD Collaboration

P. Astier [n], D. Autiero [h], A. Baldisseri [r], M. Baldo-Ceolin [m], M. Banner [n], G. Bassompierre [a], K. Benslama [i], N. Besson [r], I. Bird [h,i], B. Blumenfeld [b], F. Bobisut [m], J. Bouchez [r], S. Boyd [t], A. Bueno [c,x], S. Bunyatov [f], L. Camilleri [h], A. Cardini [j], P.W. Cattaneo [o], V. Cavasinni [p], A. Cervera-Villanueva [h,v], R. Challis [k], A. Chukanov [f], G. Collazuol [m], G. Conforto [h,u], C. Conta [o], M. Contalbrigo [m], R. Cousins [j], D. Daniels [c], H. Degaudenzi [i], T. Del Prete [p], A. De Santo [h], T. Dignan [c], L. Di Lella [h], E. do Couto e Silva [h], J. Dumarchez [n], M. Ellis [t], T. Fazio [a], G.J. Feldman [c], R. Ferrari [o], D. Ferrère [h], V. Flaminio [p], M. Fraternali [o], J.-M. Gaillard [a], E. Gangler [h,n], A. Geiser [e,h], D. Geppert [e], D. Gibin [m], S. Gninenko [h,l], A. Godley [s,t], J.-J. Gomez-Cadenas [h,v], J. Gosset [r], C. Gößling [e], M. Gouanère [a], A. Grant [h], G. Graziani [g], A. Guglielmi [m], C. Hagner [r], J. Hernando [v], D. Hubbard [c], P. Hurst [c], N. Hyett [k], E. Iacopini [g], C. Joseph [i], F. Juget [i], N. Kent [k], M. Kirsanov [l], O. Klimov [f], J. Kokkonen [h], A. Kovzelev [l,o], A. Krasnoperov [a,f], D. Kustov [f], V. Kuznetsov [f,h], S. Lacaprara [m], C. Lachaud [n], B. Lakić [w], A. Lanza [o], L. La Rotonda [d], M. Laveder [m], A. Letessier-Selvon [n], J.-M. Levy [n], L. Linssen [h], A. Ljubičić [w], J. Long [b], A. Lupi [g], A. Marchionni [g], F. Martelli [u], X. Méchain [r], J.-P. Mendiburu [a], J.-P. Meyer [r], M. Mezzetto [m], S.R. Mishra [c,s], G.F. Moorhead [k], D. Naumov [f], P. Nédélec [a], Yu. Nefedov [f], C. Nguyen-Mau [i], D. Orestano [q], F. Pastore [q], L.S. Peak [t], E. Pennacchio [u], H. Pessard [a], R. Petti [h,o], A. Placci [h], G. Polesello [o], D. Pollmann [e], A. Polyarush [l], B. Popov [f,n], C. Poulsen [k], J. Rico [x], P. Riemann [e], C. Roda [h,p], A. Rubbia [h,x], F. Salvatore [o], K. Schahmaneche [n], B. Schmidt [e,h], T. Schmidt [e], M. Sevior [k], D. Sillou [a], F.J.P. Soler [h,t], G. Sozzi [i], D. Steele [b,i], U. Stiegler [h], M. Stipčević [w], Th. Stolarczyk [r], M. Tareb-Reyes [i], G.N. Taylor [k], V. Tereshchenko [f], A. Toropin [l], A.-M. Touchard [n], S.N. Tovey [h,k], M.-T. Tran [i], E. Tsesmelis [h], J. Ulrichs [t],

0550-3213/02/$ – see front matter
PII: S0550-3213(01)00584-3

RAPID COMMUNICATION

L. Vacavant [i], M. Valdata-Nappi [d,1], V. Valuev [f,j], F. Vannucci [n], K.E. Varvell [t], M. Veltri [u], V. Vercesi [o], G. Vidal-Sitjes [h], J.-M. Vieira [i], T. Vinogradova [j], F.V. Weber [c,h], T. Weisse [e], F.F. Wilson [h], L.J. Winton [k], B.D. Yabsley [t], H. Zaccone [r], K. Zuber [e], P. Zuccon [m]

[a] *LAPP, Annecy, France*
[b] *Johns Hopkins University, Baltimore, MD, USA*
[c] *Harvard University, Cambridge, MA, USA*
[d] *University of Calabria and INFN, Cosenza, Italy*
[e] *Dortmund University, Dortmund, Germany*
[f] *JINR, Dubna, Russia*
[g] *University of Florence and INFN, Florence, Italy*
[h] *CERN, Geneva, Switzerland*
[i] *University of Lausanne, Lausanne, Switzerland*
[j] *UCLA, Los Angeles, CA, USA*
[k] *University of Melbourne, Melbourne, Australia*
[l] *Institute of Nuclear Research, INR Moscow, Russia*
[m] *University of Padova and INFN, Padova, Italy*
[n] *LPNHE, University of Paris VI and VII, Paris, France*
[o] *University of Pavia and INFN, Pavia, Italy*
[p] *University of Pisa and INFN, Pisa, Italy*
[q] *Roma Tre University and INFN, Rome, Italy*
[r] *DAPNIA, CEA Saclay, France*
[s] *University of South Carolina, Columbia, SC, USA*
[t] *University of Sydney, Sydney, Australia*
[u] *University of Urbino, Urbino, and INFN Florence, Italy*
[v] *IFIC, Valencia, Spain*
[w] *Rudjer Bošković Institute, Zagreb, Croatia*
[x] *ETH Zürich, Zürich, Switzerland*

Received 1 November 2001; accepted 14 November 2001

Abstract

A study of strange particle production in ν_μ charged current interactions has been performed using the data from the NOMAD experiment. Yields of neutral strange particles (K^0_S, Λ, $\bar{\Lambda}$) have been measured. Mean multiplicities are reported as a function of the event kinematic variables E_ν, W^2 and Q^2 as well as of the variables describing particle behaviour within a hadronic jet: x_F, z and p_T^2. Decays of resonances and heavy hyperons with identified K^0_S and Λ in the final state have been analyzed. Clear signals corresponding to $K^{\star\pm}$, $\Sigma^{\star\pm}$, Ξ^- and Σ^0 have been observed.

Keywords: Neutrino interactions; Strange particle production

1. Introduction

The production of strange particles in neutrino interactions can provide a testing ground for the quark–parton as well as for hadronization models. Neutral strange particles can be

E-mail address: popov@nusun.jinr.dubna.su (B. Popov).

[1] Now at University of Perugia and INFN, Perugia, Italy.

reliably identified using the V^0-like signature of their decays ($K^0_s \to \pi^+\pi^-$, $\Lambda \to p\pi^-$ and $\bar{\Lambda} \to \bar{p}\pi^+$) in contrast to most other hadrons which require particle identification hardware. It is noteworthy that all previous investigations of strange particle production by neutrinos have come from bubble chamber experiments [1–25]. No other technique has so far yielded results on this subject. However, previous bubble chamber experiments with (anti)neutrino beams suffered from the low statistics of their V^0 samples.

The NOMAD experiment [26] has collected a large number of neutrino interactions with a reconstruction quality similar to that of bubble chamber experiments. The order of magnitude increase in statistics can be used to improve our knowledge of strange particle production in neutrino interactions. In this paper we present measurements of the yields of neutral strange particles (K^0_s, Λ and $\bar{\Lambda}$), as well as the yields of $K^{\star\pm}$, $\Sigma^{\star\pm}$, Ξ^- and Σ^0 in ν_μ charged current (CC) interactions. These results are compared to the predictions of the NOMAD Monte Carlo (MC) simulation program.

The results of the present analysis are the measurements of:

(1) the production properties of neutral strange particles in ν_μ CC interactions. This study will allow tuning of the parameters of the MC simulation programs in order to correctly reproduce the production of strange particles by neutrinos;
(2) the contribution of strange resonances and heavy hyperons to the total number of observed K^0_s, Λ and $\bar{\Lambda}$. This will allow a quantitative theoretical interpretation of the Λ and $\bar{\Lambda}$ polarization measurements in ν_μ CC deep inelastic scattering (DIS) reported in our previous articles [27,28].

2. Experimental procedure

2.1. The NOMAD experiment

The main goal of the NOMAD experiment [26] was the search for $\nu_\mu \to \nu_\tau$ oscillations in a wide-band neutrino beam from the CERN SPS. The main characteristics of the beam are given in Table 1. This search uses kinematic criteria to identify ν_τ CC interactions [29] and requires a very good quality of event reconstruction similar to that of bubble chamber experiments. This has indeed been achieved by the NOMAD detector, and, moreover,

Table 1
The CERN SPS neutrino beam composition at the position of the NOMAD detector (as predicted by the beam simulation program [35])

Neutrino	Flux		CC interactions in NOMAD	
flavours	$\langle E_\nu \rangle$ (GeV)	Rel. abund.	$\langle E_\nu \rangle$ (GeV)	Rel. abund.
ν_μ	24.2	1	45.3	1
$\bar{\nu}_\mu$	18.5	0.0637	40.9	0.0244
ν_e	36.6	0.0102	57.1	0.0153
$\bar{\nu}_e$	28.7	0.0025	49.9	0.0015

the large data sample collected during four years of data taking (1995–1998) allows for a detailed study of neutrino interactions. The full data sample from the NOMAD experiment corresponding to about 1.3 million ν_μ CC interactions in the detector fiducial volume is used in the present analysis. The data are compared to the results of a Monte Carlo simulation based on modified versions of LEPTO 6.1 [30] and JETSET 7.4 [31] generators for neutrino interactions (with Q^2 and W^2 cutoff parameters removed) and on a GEANT [32] based program for the detector response. Strange particle production is described by the set of default parameters in JETSET. To define the parton content of the nucleon for the cross-section calculation we have used the GRV-HO parametrization [33] of the parton density functions available in PDFLIB [34]. The above description of the MC will be referred to as the default MC. For the analysis reported below we used a MC sample consisting of about 3 million events.

2.2. The NOMAD detector

For a study of strange particle production the tracking capabilities of a detector are of paramount importance. The NOMAD detector (Fig. 1) is especially well suited for this. It consists of an active target of 44 drift chambers, with a total fiducial mass of 2.7 tons, located in a 0.4 Tesla dipole magnetic field. The drift chambers (DC) [36], made of low Z material (mainly carbon) serve the dual role of a nearly isoscalar target for neutrino interactions and of the tracking medium. The average density of the drift chamber volume is 0.1 g/cm^3, very close to that of liquid hydrogen. These drift chambers provide an overall efficiency for charged particle reconstruction of better than 95% and a momentum

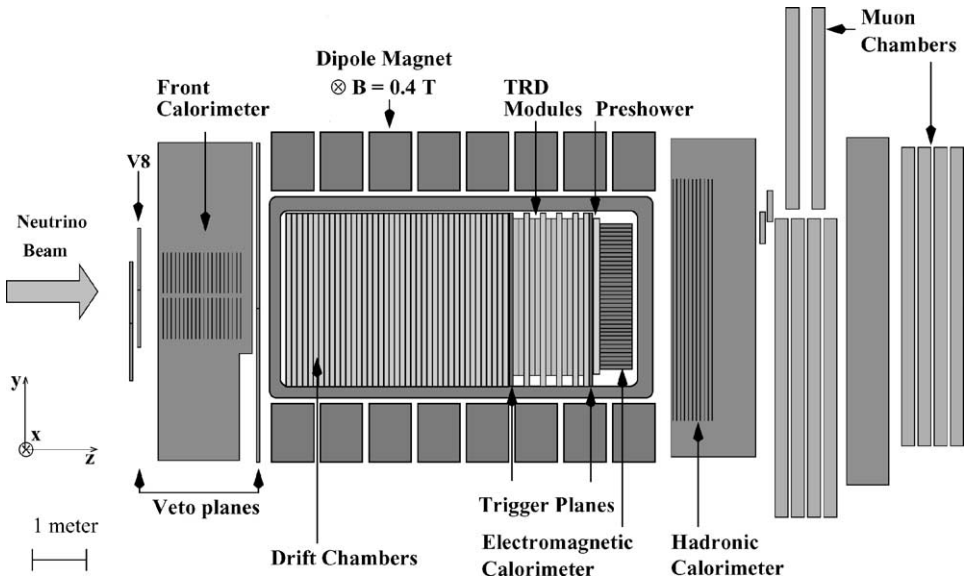

Fig. 1. A sideview of the NOMAD detector.

resolution which can be parametrized as

$$\frac{\sigma_p}{p} = \frac{0.05}{\sqrt{L}} \oplus \frac{0.008 \cdot p}{\sqrt{L^5}},$$

where the track length L is in meters and the track momentum p is in GeV/c. This amounts to a resolution of approximately 3.5% in the momentum range of interest (less than 10 GeV/c). Reconstructed tracks are used to determine the event topology (the assignment of tracks to vertices), to reconstruct the vertex position and the track parameters at each vertex and, finally, to identify the vertex type (primary, secondary, V^0, etc.). A transition radiation detector [37] is used for electron identification. The pion rejection achieved for isolated tracks is 10^3 with a 90% electron identification efficiency. A lead-glass electromagnetic calorimeter [38] located downstream of the tracking region provides an energy resolution of $3.2\%/\sqrt{E\ [\mathrm{GeV}]} \oplus 1\%$ for electromagnetic showers and is essential to measure the total energy flow in neutrino interactions. In addition, an iron absorber and a set of muon chambers located after the electromagnetic calorimeter are used for muon identification, providing a muon detection efficiency of 97% for momenta greater than 5 GeV/c.

The large statistics of the data combined with the good quality of event reconstruction in the NOMAD detector allows a detailed study of strange particle production in neutrino interactions to be performed.

2.3. Event selection and V^0 identification procedure

The NOMAD experiment has collected 1.3×10^6 ν_μ CC events and has observed an unprecedented number of neutral strange particle decays. Such a decay appears in the detector as a V^0-like vertex: two tracks of opposite charge emerging from a common vertex separated from the primary neutrino interaction vertex (Fig. 2). The V^0-like signature is expected also for photon conversions.

The selection procedure for the ν_μ CC event sample used in this analysis has been described in [27].

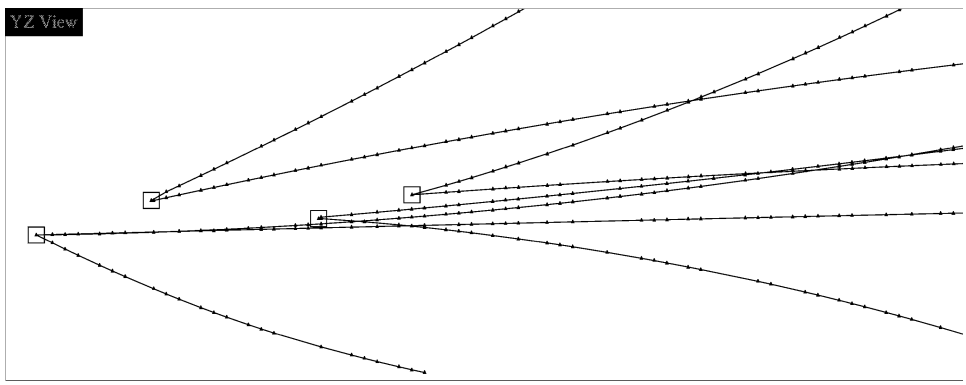

Fig. 2. A reconstructed data event containing 3 V^0 vertices identified as K^0_S decays by our identification procedure. The scale on this plot is given by the size of the vertex boxes (3×3 cm^2).

Since the NOMAD detector is unable to distinguish (anti)protons from pions in the momentum range relevant to this analysis, our V^0 identification procedure relies on the kinematic properties of a V^0 decay.

For the V^0 identification a kinematic fit method has been used as described in [27,39]. This fit has been performed for three decay hypotheses: $K^0_s \to \pi^+\pi^-$, $\Lambda \to p\pi^-$, $\bar{\Lambda} \to \bar{p}\pi^+$ and for the hypothesis of a photon conversion to e^+e^-. The output of the kinematic fits applied to a given V^0 vertex consists of four values of $\chi^2_{V^0}$ describing the goodness of these fits. Different regions in the four-dimensional $\chi^2_{V^0}$ space populated by particles identified as K^0_s, Λ and $\bar{\Lambda}$ have been selected. Identified V^0 are of two types:

- *uniquely* identified V^0, which, in the four-dimensional $\chi^2_{V^0}$ space described above, populate regions in which decays of only a single particle type are present;
- *ambiguously* identified V^0, which populate regions in which decays of different particle types are present.

The treatment of ambiguities aims at selecting a given V^0 decay with the highest efficiency and the lowest background contamination from other V^0 types. An optimum compromise between high statistics of the identified V^0 sample and well understood background contamination is the aim of our identification strategy. The MC simulation program has been used to define the criteria for the kinematic V^0 selection and to determine the purity of the final K^0_s, Λ and $\bar{\Lambda}$ samples. We selected a sample consisting of more than 90% of uniquely identified V^0. Results are reported in Table 2.

The total V^0 sample in our data contains 15074 identified K^0_s, 8087 identified Λ and 649 identified $\bar{\Lambda}$ decays, representing significantly larger numbers than in previous (anti)neutrino experiments performed with bubble chambers [1–25].

Fig. 3 shows the invariant mass and $c\tau$ distributions for identified K^0_s, Λ and $\bar{\Lambda}$. The measured mass and the lifetime of identified neutral strange particles are in agreement with the world averages [40]. The corresponding results are given in Tables 3 and 4.

The efficiencies and purities reported in Table 2 are momentum dependent. However, we have checked that they are applicable to the data because the momenta distributions of identified V^0 and of their decay products are very similar in the data and MC simulation.

In the rest of this paper we will always present efficiency corrected distributions.

Table 2
Efficiency (ϵ) and purity (P) for each selected V^0 category. Numbers of identified neutral strange particles in the data are also shown in the last column

V^0	ϵ (%)	P (%)	Data
K^0_s	22.1 ± 0.1	97.2 ± 0.1	15074
Λ	16.4 ± 0.1	95.9 ± 0.1	8087
$\bar{\Lambda}$	18.6 ± 0.5	89.7 ± 0.7	649

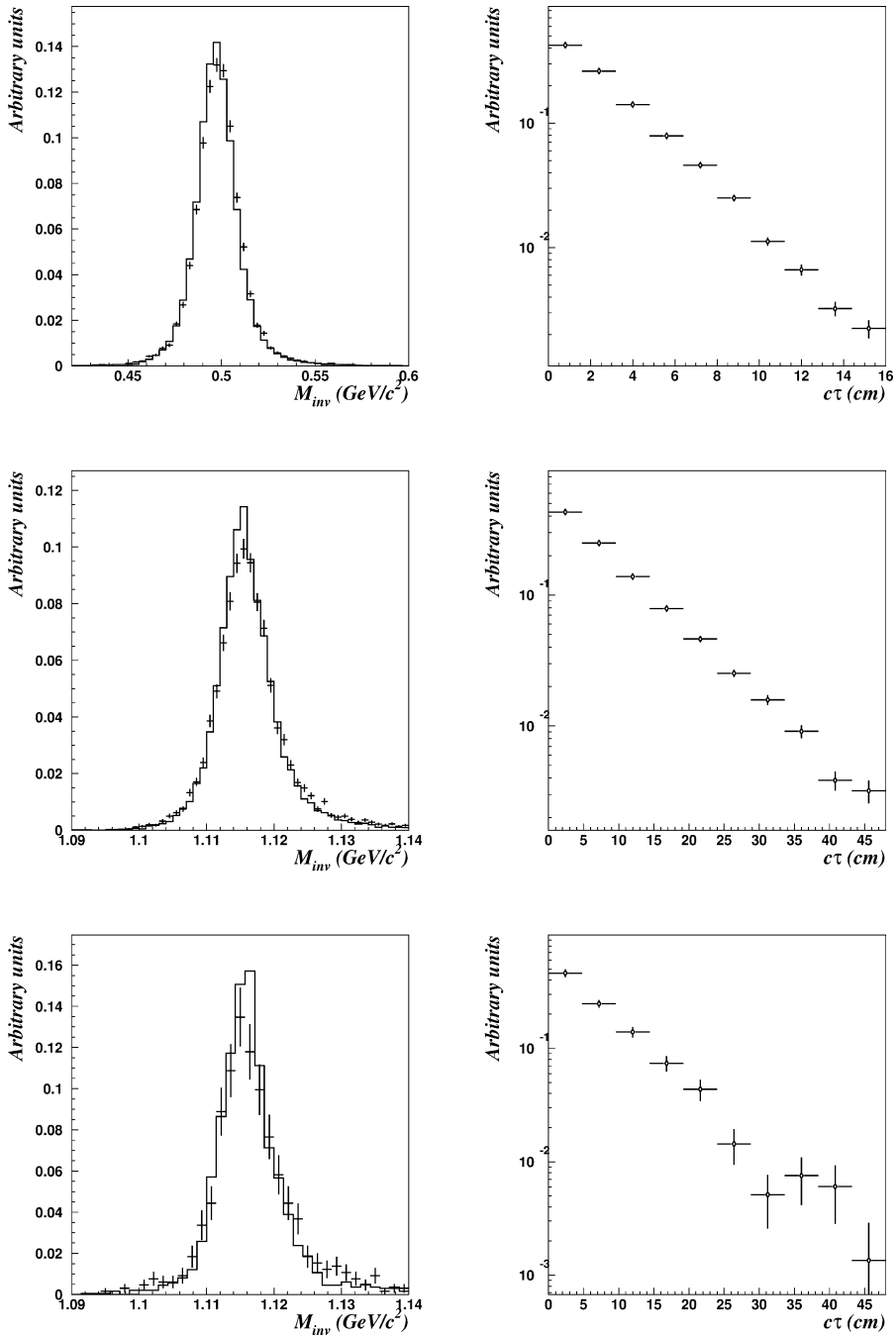

Fig. 3. Invariant mass distributions and efficiency corrected $c\tau$ distributions for identified K^0_S (top), Λ (center) and $\bar{\Lambda}$ (bottom) in ν_μ CC DIS events for both data (points with error bars) and MC (histogram).

Table 3
Measured V^0 mass and resolution (in MeV/c^2) for both MC and data

V^0	MC		Data		PDG[40]
	Mass	Resolution	Mass	Resolution	Mass
K^0_S	497.9 ± 0.1	11.0 ± 0.1	497.9 ± 0.1	11.3 ± 0.1	497.672 ± 0.031
Λ	1115.7 ± 0.02	4.0 ± 0.03	1116.0 ± 0.05	4.45 ± 0.05	1115.683 ± 0.006
$\bar{\Lambda}$	1116.0 ± 0.1	4.1 ± 0.1	1116.3 ± 0.1	4.8 ± 0.2	1115.683 ± 0.006

Table 4
Measured $c\tau$ (in cm) for a given V^0 type for both MC and data

V^0	MC	Data	PDG [40]
K^0_S	2.60 ± 0.01	2.72 ± 0.03	2.6786
Λ	7.91 ± 0.02	8.07 ± 0.12	7.89
$\bar{\Lambda}$	7.82 ± 0.06	7.33 ± 0.33	7.89

3. Yields of neutral strange particles

We have studied the production rates of neutral strange particles (K^0_S, Λ, $\bar{\Lambda}$) in ν_μ CC interactions. The particles can be produced at the primary vertex and also from secondary interactions of primary particles with the detector material. Neutral strange particles produced via resonance or heavier hyperon decays are classified as primary V^0. We applied a correction obtained from the Monte Carlo to the yields of neutral strange particles in the data in order to extract the yields at the primary vertex.

3.1. Integral yields of neutral strange particles

The measured yield per ν_μ CC interaction for each V^0 type is defined as:

$$T_{V^0} = \xi \cdot \frac{N_{V^0}}{N_{\nu_\mu \mathrm{CC}}}, \tag{1}$$

where N_{V^0} is the number of reconstructed and identified V^0 in the number $N_{\nu_\mu \mathrm{CC}}$ of reconstructed ν_μ CC events and ξ is a correction factor calculated as:

$$\xi = \frac{P_{V^0} \times \epsilon_{\nu_\mu \mathrm{CC}}}{\epsilon_{V^0} \times Br(V^0 \to h^+h^-)},$$

where $\epsilon_{\nu_\mu \mathrm{CC}} = (85.30 \pm 0.02)\%$ is the efficiency (reconstruction and identification) of ν_μ CC events in the fiducial volume, and ϵ_{V^0} is the global V^0 efficiency which takes into account the contribution from particles produced in the fiducial volume, but decaying outside. P_{V^0} is the purity of the final V^0 sample, and $Br(V^0 \to h^+h^-)$ is the branching ratio for a given V^0 type decaying to a pair of charged hadrons.

Table 5
Integral yields of primary V^0 in ν_μ CC interactions in both the data and in the default MC. The errors are only statistical

V^0 type	$T_{V^0}^{\mathrm{DATA}}$ (%)	$T_{V^0}^{\mathrm{MC}}$ (%)	$T_{V^0}^{\mathrm{MC}}/T_{V^0}^{\mathrm{DATA}}$
K_s^0	6.76 ± 0.06	9.50 ± 0.02	1.40 ± 0.01
Λ	5.04 ± 0.06	8.10 ± 0.02	1.61 ± 0.02
$\bar{\Lambda}$	0.37 ± 0.02	0.60 ± 0.01	1.62 ± 0.03

Table 5 shows the overall inclusive production rates for K_s^0, Λ and $\bar{\Lambda}$ in ν_μ CC interactions compared to the MC predictions. Note that the production rates in the default MC are a factor of 1.4 to 1.6 higher than in the data. This could be explained in part by the choice of the LEPTO [30] and JETSET [31] parameters in the NOMAD event generator. We have to emphasize that the so-called $s\bar{s}$ suppression factor (PARJ(2) parameter in JETSET)—defined as the ratio of the probability γ_s of producing an $s\bar{s}$ pair to the probability γ_u (γ_d) of producing a $u\bar{u}$ ($d\bar{d}$) pair in the fragmentation chain—was set to its default value of 0.3 in the default NOMAD MC production.[2] However, this parameter was measured to be about 0.2 in previous bubble chamber experiments: for example, the values obtained by the BEBC WA21 Collaboration [41] in a neutrino beam similar to ours are $0.200 \pm 0.022(\mathrm{stat}) \pm 0.010(\mathrm{sys})$ for $\bar{\nu}p$ and $0.207 \pm 0.018(\mathrm{stat}) \pm 0.020(\mathrm{sys})$ for νp interactions. Moreover, later results from OPAL (0.245) [42], DELPHI (0.23) [43], E665 (0.2) [44], ZEUS [45] and H1 [46] Collaborations support a value close to 0.2 for this parameter.

However, the problem of the inaccurate description of neutral strange particle production in the MC is a more complex one. This is illustrated in Table 6, where we give the observed numbers of ν_μ CC events for 10 exclusive multi-V^0 channels in the data compared to the default MC predictions. The number of MC events in Table 6 is renormalized to the same number of ν_μ CC events as in the data. From this comparison one can conclude that it is not possible to rescale just a single parameter (the $s\bar{s}$ suppression factor) in order to describe the neutral strange particle production observed in the data. Rather, the discrepancy is due to a combination of several parameters which describe the probability that an $s(\bar{s})$-quark appears as a meson/baryon(antibaryon), the probability that a strange meson/baryon(antibaryon) appears electrically neutral, etc. A tuning of the JETSET parameters to reproduce the yields of neutral strange particles observed in the NOMAD data is a subject of an analysis currently in progress.

The integral yields reported in Table 5 can be compared to previous measurements summarized in Table 7. The K_s^0 rates from Table 5 have been converted into $K^0 (= K^0 + \overline{K}^0)$ rates by multiplying by a factor of 2.

For completeness we have recalculated the integral overall yields taking into account contributions from both primary and secondary V^0. These results are given in Table 7

[2] The value 0.3 has been suggested by the authors of JETSET as the default for this parameter.

Table 6
Numbers of ν_μ CC events with a specified combination of observed neutral strange particle decays for both the default MC and data. X indicates the hadronic system accompanying the observed V^0

	Number of observed events		
Channel	MC	Data	MC/DATA
ΛX	11686	7778	1.50 ± 0.02
$K^0_s X$	18971	14228	1.33 ± 0.01
$\bar{\Lambda} X$	831	594	1.40 ± 0.07
$K^0_s K^0_s X$	485	284	1.7 ± 0.1
$\Lambda K^0_s X$	617	247	2.5 ± 0.2
$\Lambda \bar{\Lambda} X$	98	40	2.5 ± 0.4
$K^0_s \bar{\Lambda} X$	24	15	1.6 ± 0.5
$\Lambda \Lambda X$	19	10	1.9 ± 0.7
$\Lambda K^0_s K^0_s X$	7	2	3.4 ± 2.6
$K^0_s K^0_s K^0_s X$	2	4	0.6 ± 0.4

Table 7
Inclusive yields of neutral strange particles in ν_μ CC interactions measured in this analysis and in previous bubble chamber experiments. N_K, N_Λ and $N_{\bar{\Lambda}}$ are the observed numbers of K^0_s, Λ and $\bar{\Lambda}$, respectively. K^0 stands for $K^0 + \bar{K}^0$. See text for explanation of a star ($\star$)

Reaction [Ref.]	$\langle E_\nu \rangle$ (GeV)	$N_{K^0_s}$	K^0 rate (%)	N_Λ	Λ rate (%)	$N_{\bar{\Lambda}}$	$\bar{\Lambda}$ rate (%)
NOMAD	45	15075	13.52 ± 0.12	8087	5.04 ± 0.06	649	0.37 ± 0.02
NOMAD*	45	15075	18.22 ± 0.16	8087	6.66 ± 0.08	649	0.45 ± 0.02
ν–Ne [19]	46	2279	16.8 ± 1.2	1843	6.5 ± 0.5	93	0.46 ± 0.08
ν–p [24]	51	831	19.0 ± 0.9	491	5.2 ± 0.3	27	0.34 ± 0.07
ν–Ne [25]	150	502	40.8 ± 4.8	285	12.7 ± 1.4	27	1.5 ± 0.5
ν–p [11]	43	359	17.5 ± 0.9	180	4.5 ± 0.4	13	0.3 ± 0.1
ν–Ne [12]	103	203	23.0 ± 1.7	98	5.7 ± 0.7		
ν–n [14]	62	234	20.8 ± 1.6	157	7.1 ± 0.7		
ν–p [14]	62	154	17.7 ± 1.6	77	4.3 ± 0.6		
ν–n [17]	62		20.5 ± 1.1		6.6 ± 0.7		
ν–p [17]	62		17.4 ± 1.2		4.4 ± 0.5		
ν–A [21]	$\sim$10	82	7.1 ± 0.8	76	3.1 ± 0.4		
ν–p [10]	$\sim$45	23	15 ± 4				
ν–p [15]	$\sim$50				7.0 ± 0.8		
ν–n [15]	$\sim$50				7.0 ± 1.2		

and denoted by a star ($\star$). Our overall yields are consistent with the results of the ν–Ne experiment [19] performed in a similar neutrino beam. However, our primary yields of K^0_s and Λ are about 30% lower and the primary yield of $\bar{\Lambda}$ is $\sim$20% lower.

3.2. Yields of neutral strange particles as a function of kinematic variables

To investigate neutral strange particle production mechanisms we have measured the average K^0_S, Λ and $\bar{\Lambda}$ yields as a function of the neutrino energy E_ν, the invariant effective mass squared W^2 of the hadronic system, the invariant square of the four-momentum transfer from the neutrino to the target Q^2, and the Bjorken scaling variable x_{Bj}.

The yields of K^0_S, Λ and $\bar{\Lambda}$ are shown in Fig. 4. The Λ yield shows a behaviour which is almost independent of E_ν, W^2 and Q^2 after a sharp initial rise. It drops at large values of x_{Bj}. On the other hand, the yield of K^0_S rises steadily with E_ν and W^2, reaches a plateau at large Q^2 and falls with increasing x_{Bj}. Similar observations have been made by previous experiments, but with larger statistical uncertainties. The $\bar{\Lambda}$ yields as a function of kinematic variables are measured for the first time in a neutrino experiment. In general

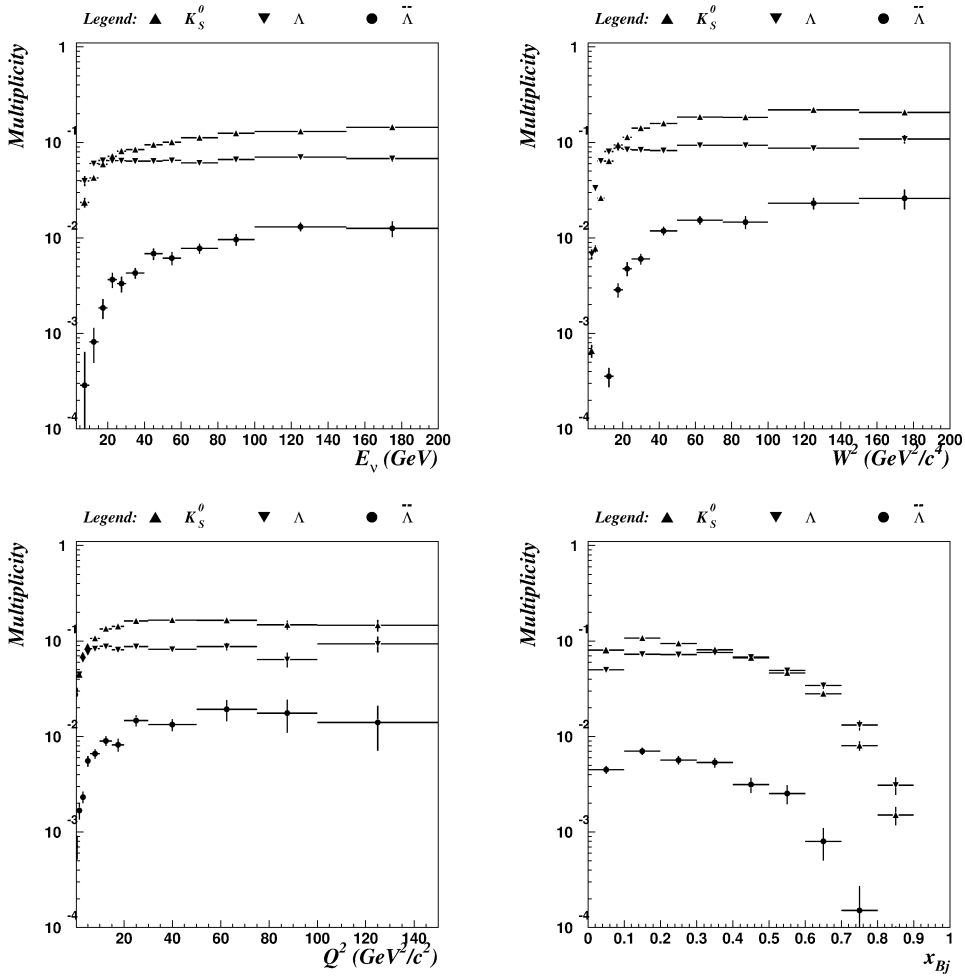

Fig. 4. Measured yields of the K^0_S, Λ and $\bar{\Lambda}$ as a function of E_ν, W^2, Q^2 and x_{Bj}.

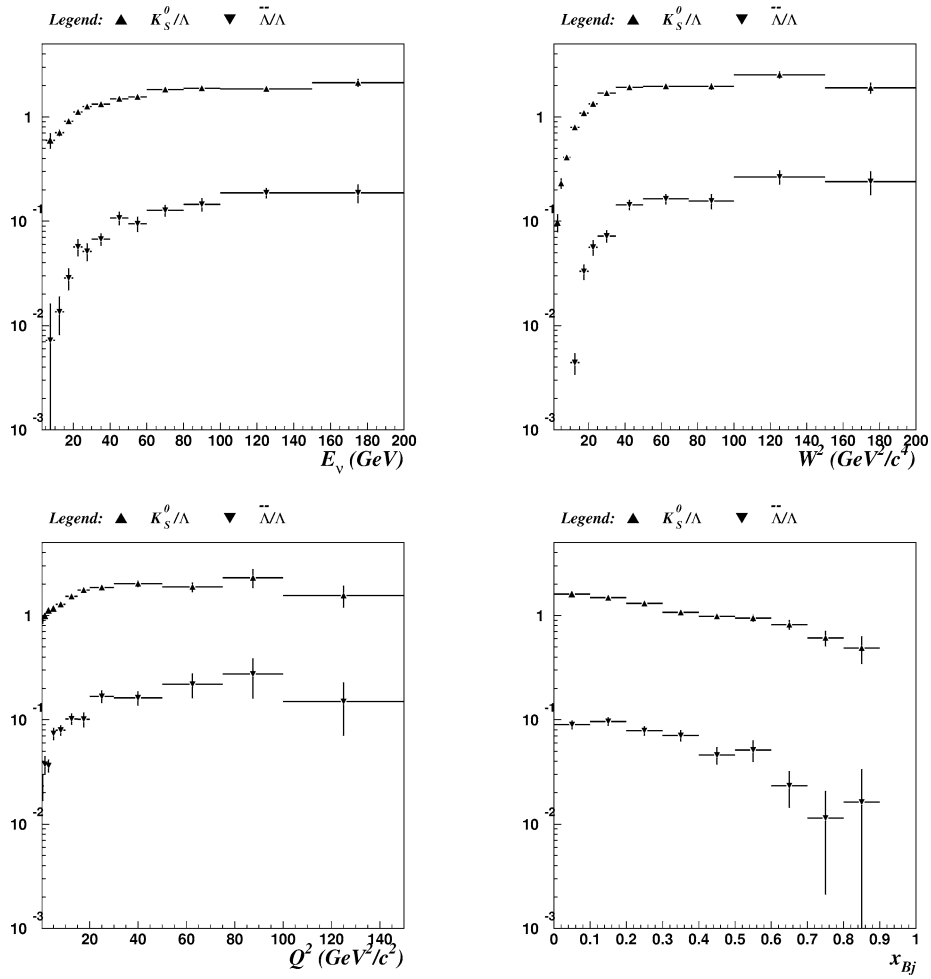

Fig. 5. Ratios of measured yields for K^0_S/Λ and $\bar{\Lambda}/\Lambda$ as a function of E_ν, W^2, Q^2 and x_{Bj}.

they show a behaviour similar to that of the K^0_S. However, as expected, clear W^2 and E_ν thresholds are present in the $\bar{\Lambda}$ production.

The ratios of yields for K^0_S/Λ and $\bar{\Lambda}/\Lambda$ are presented in Fig. 5.

3.3. Comparison with LUND model predictions

The measured yields of K^0_S, Λ and $\bar{\Lambda}$ particles are compared in Figs. 6–8 to the predictions of the default NOMAD MC simulation (see Section 2.1). A reasonable agreement in shapes is observed, while the discrepancy in the overall normalization is about a factor of 1.3 to 1.5.

The kinematic variables E_ν, W^2, Q^2 and x_{Bj} are not independent. So, for example, discrepancies between the data and MC at high W^2 are reflected in discrepancies at low x_{Bj}.

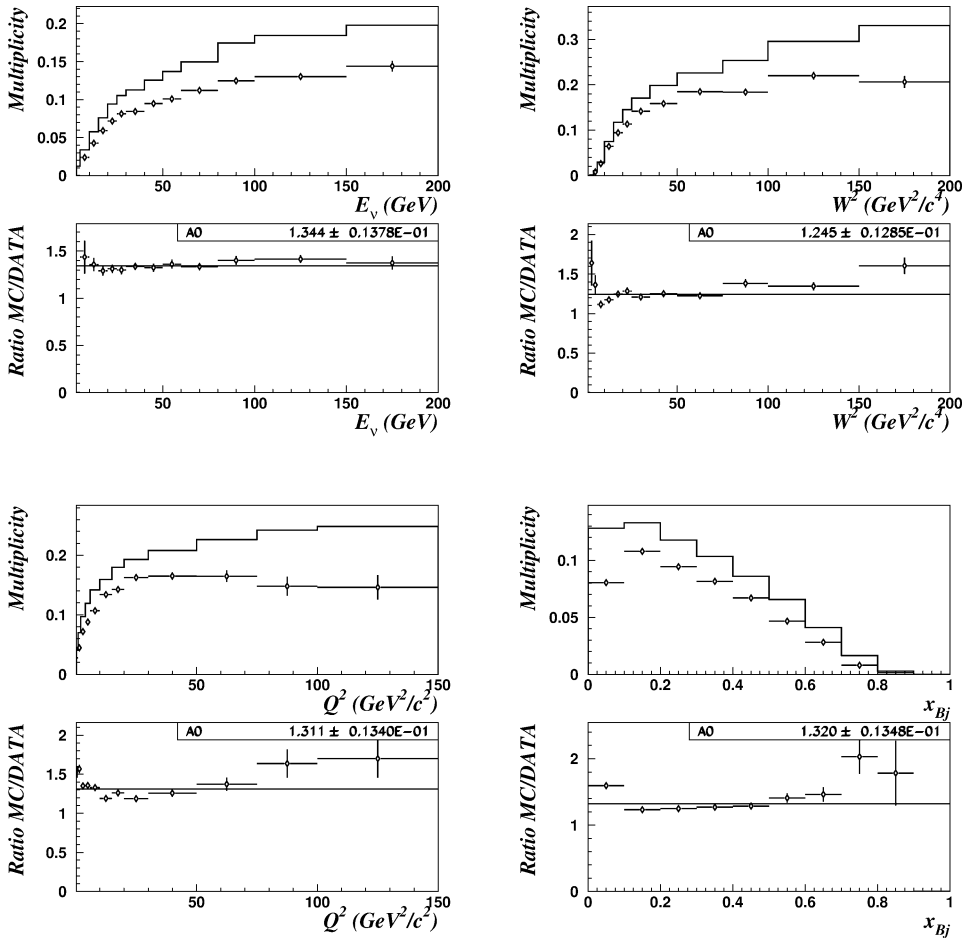

Fig. 6. Yields in the default MC (histogram) and in the data (points with error bars) for K^0_S as a function of E_ν, W^2, Q^2 and x_{Bj}. The MC/Data ratios and their fit to a constant are also shown.

4. Production properties

We have also performed a detailed analysis of kinematic quantities describing the behaviour of neutral strange particles (K^0_S, Λ and $\bar{\Lambda}$) inside the hadronic jet. This study allows an investigation of the dynamics of fragmentation. The differences in the production properties of K^0_S, Λ and $\bar{\Lambda}$ are seen most clearly here. The following distributions are of interest: $x_F = 2p^*_L/W$ (Feynman-x is the longitudinal momentum fraction in the hadronic center of mass system), the transverse momentum squared, p^2_T, of a particle with respect to the current (hadronic jet) direction and the fraction $z = E_{\mathrm{lab}}(V^0)/E_{\mathrm{lab}}$ (all hadrons) of the total hadronic energy carried away by the neutral strange particle in the laboratory system.

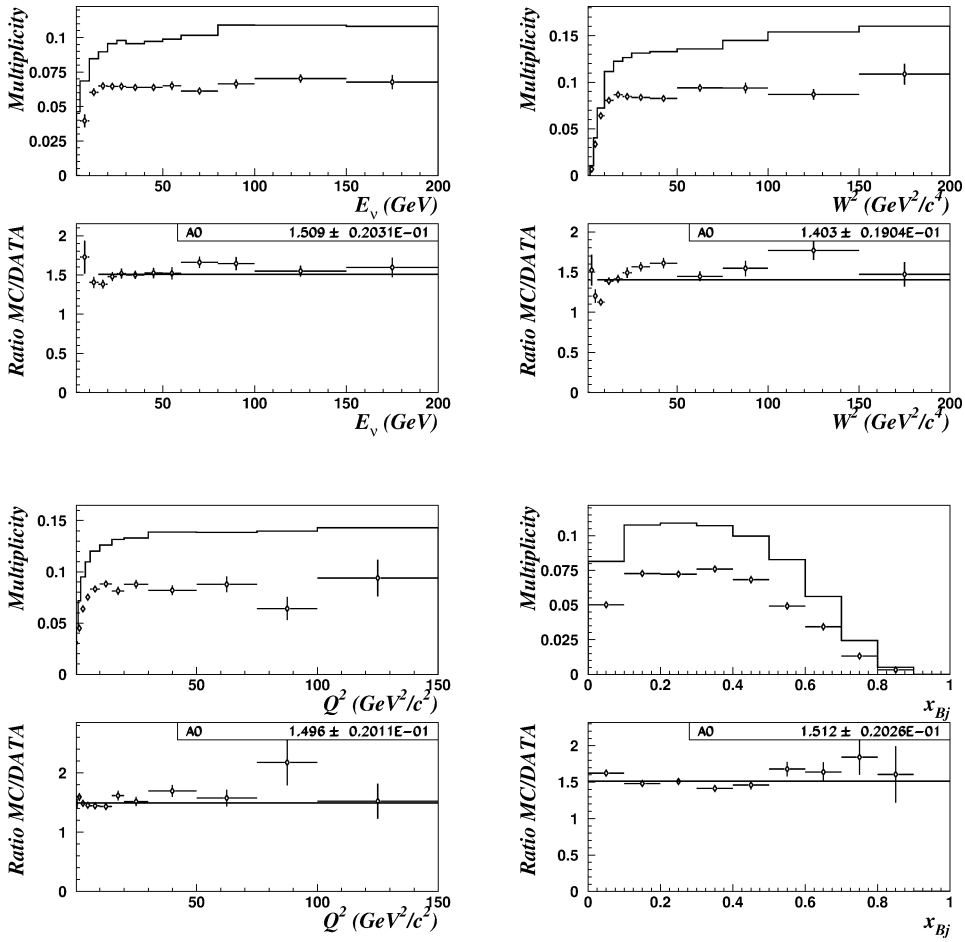

Fig. 7. Yields in the default MC (histogram) and in the data (points with error bars) for Λ as a function of E_ν, W^2, Q^2 and x_{Bj}. The MC/Data ratios and their fit to a constant are also shown.

4.1. x_F distributions

The efficiency corrected x_F distributions observed in the data for neutral strange particles are shown in Figs. 9–11. These distributions indicate that Λ are produced mainly in the target fragmentation region ($x_F < 0$), while $\mathrm{K}^0_{\mathrm{s}}$ are peaked in the central region with an asymmetry in the forward direction. $\bar{\Lambda}$ are produced in the central x_F region ($|x_F| < 0.5$). One way to quantify differences in the x_F distributions is to define an asymmetry parameter $A = (N_F - N_B)/(N_F + N_B)$, where N_F and N_B are the numbers of particles produced forward and backward, respectively, in the hadronic center of mass. The asymmetry parameters A and mean values of x_F in both data and MC are listed in Table 8. They are consistent with previous measurements [11,12,14,19,23–25]. The observed disagreement between data and MC is probably due to the fact that the MC simulation does not properly describe the relative contributions of different V^0 production

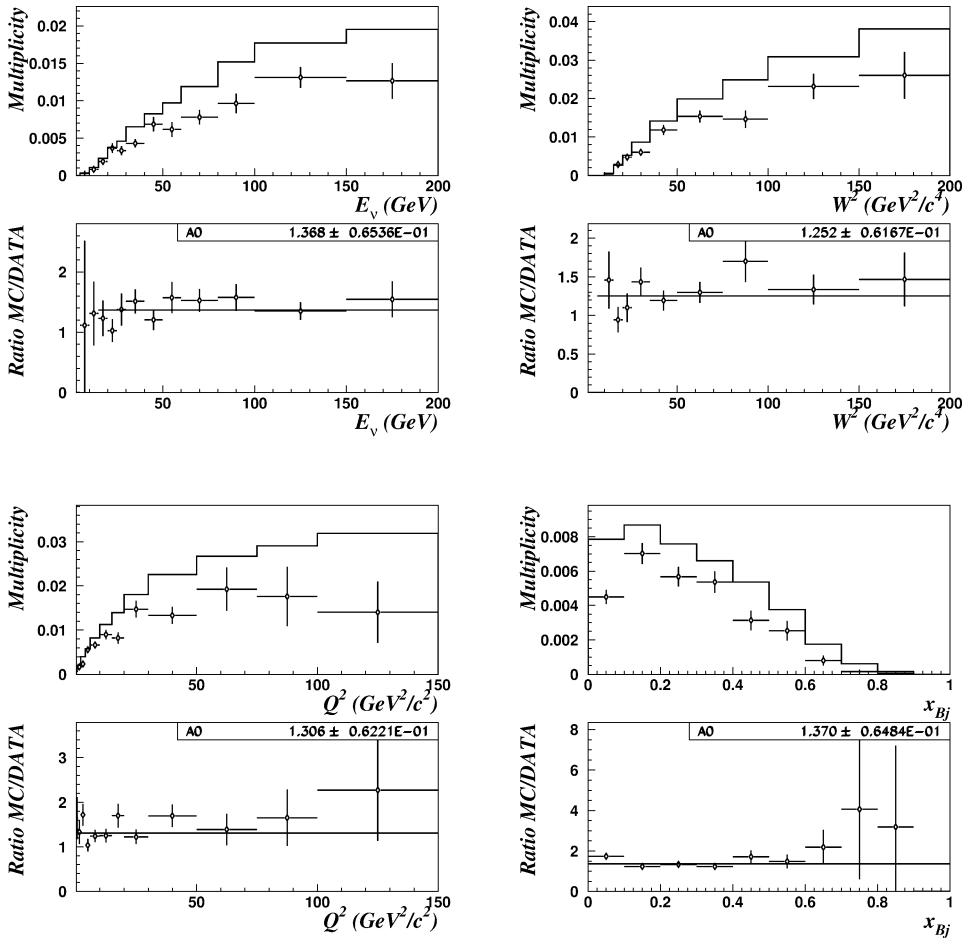

Fig. 8. Yields in the default MC (histogram) and in the data (points with error bars) for $\bar{\Lambda}$ as a function of E_ν, W^2, Q^2 and x_{Bj}. The MC/Data ratios and their fit to a constant are also shown.

mechanisms.

4.2. z distributions

Efficiency corrected z distributions for K^0_s, Λ and $\bar{\Lambda}$ are shown in Figs. 12–14. A turn-over at small values of z can be seen for $\bar{\Lambda}$ hyperons, but not for K^0_s and Λ. A turn-over at small values of z for K^0_s and Λ was observed in some of the previous neutrino experiments [8,11,14,21] and was not observed in others [10,12]. We note that uncorrected z distributions show such a turn-over for all V^0 types in our experiment as well, due to a less efficient V^0 reconstruction at low momenta.

Below we study separately z distributions of neutral strange particles produced at $x_F < 0$ (see Section 4.2.1) and at $x_F > 0$ (see Section 4.2.2). Detailed information on the mean values of z distributions for both data and MC is given in Table 9.

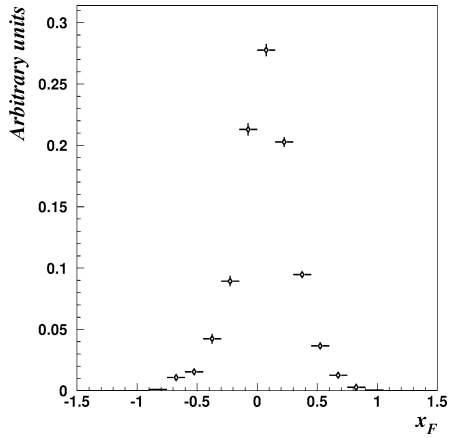

Fig. 9. Efficiency corrected x_F distribution for K^0_s mesons.

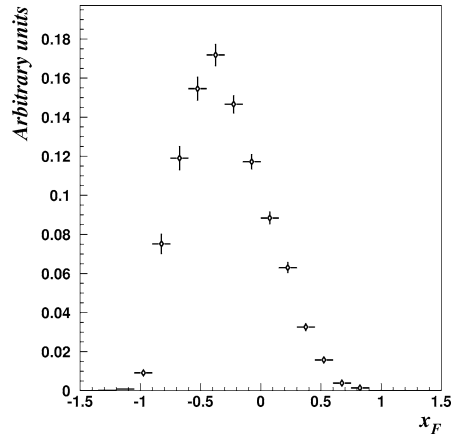

Fig. 10. Efficiency corrected x_F distribution for Λ hyperons.

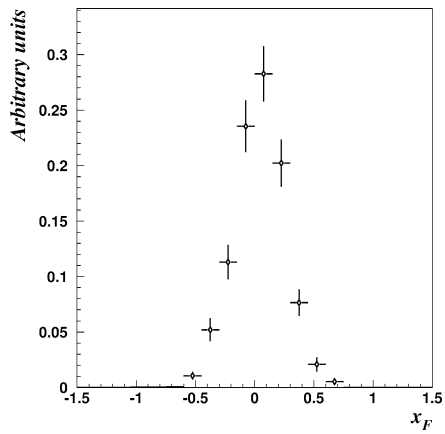

Fig. 11. Efficiency corrected x_F distribution for $\bar{\Lambda}$ hyperons.

Table 8
Mean values $\langle x_F \rangle$ and asymmetry parameters A of the x_F distributions for K^0_s, Λ, $\bar{\Lambda}$ in both MC and data

V^0	MC		DATA	
	$\langle x_F \rangle$	A	$\langle x_F \rangle$	A
K^0_s	0.055 ± 0.001	0.152 ± 0.002	0.064 ± 0.001	0.256 ± 0.004
Λ	-0.296 ± 0.001	-0.649 ± 0.002	-0.295 ± 0.002	-0.589 ± 0.004
$\bar{\Lambda}$	0.006 ± 0.002	-0.03 ± 0.01	0.04 ± 0.004	0.18 ± 0.02

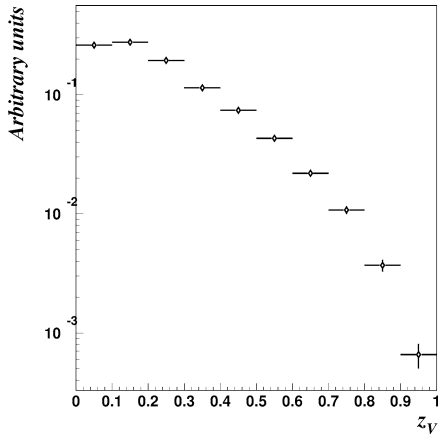

Fig. 12. Efficiency corrected z distribution for K^0_s mesons.

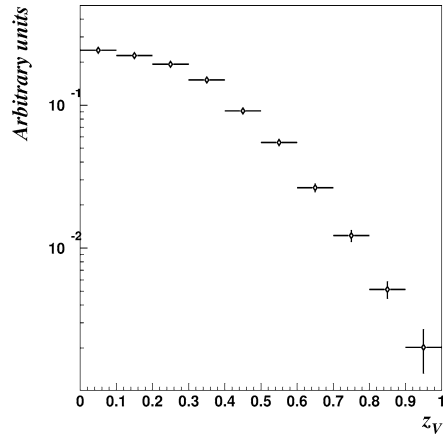

Fig. 13. Efficiency corrected z distribution for Λ hyperons.

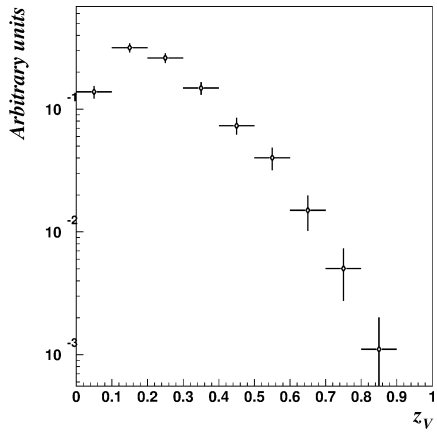

Fig. 14. Efficiency corrected z distributions for $\bar{\Lambda}$.

Table 9
Mean values of z distributions for K^0_s, Λ, $\bar{\Lambda}$ measured for the full sample and for $x_F < 0$ and $x_F > 0$ regions in both MC and data

V^0		Full sample	$x_F < 0$	$x_F > 0$
K^0_s	MC	0.218 ± 0.001	0.092 ± 0.001	0.312 ± 0.001
	DATA	0.226 ± 0.001	0.105 ± 0.001	0.299 ± 0.001
Λ	MC	0.227 ± 0.001	0.179 ± 0.001	0.462 ± 0.003
	DATA	0.250 ± 0.002	0.206 ± 0.001	0.434 ± 0.005
$\bar{\Lambda}$	MC	0.215 ± 0.003	0.139 ± 0.002	0.296 ± 0.004
	DATA	0.242 ± 0.005	0.147 ± 0.005	0.308 ± 0.008

4.2.1. z distributions in the target fragmentation region

The efficiency corrected z distributions of K^0_s, Λ and $\bar{\Lambda}$ measured in the target fragmentation region are shown in Fig. 15 (left). One can see that the z distribution of K^0_s mesons has a maximum at $z \to 0$ and decreases faster at larger z (compared with Fig. 12) and that the K^0_s mesons produced in the target fragmentation region carry in general a small fraction of the hadronic jet energy. Λ hyperons are believed to be produced mostly from the remnant di-quark fragmentation and the shape of the z distribution is similar to that shown in Fig. 13. The turn-over in the z distribution is observed for $\bar{\Lambda}$ hyperons produced in the target fragmentation region.

4.2.2. z distributions in the current fragmentation region

The efficiency corrected z distributions of K^0_s, Λ and $\bar{\Lambda}$ measured in the current fragmentation region are shown in Fig. 15 (right). This kinematical region is interesting because of the u or $\bar{d}$ (anti)quark fragmentation into Λ or $\bar{\Lambda}$ hyperons. All three z distributions show similar behaviour but with different mean values of z. The z distribution of Λ hyperons at $x_F > 0$ is drastically different from that in the target fragmentation region. This is evidence for the fragmentation of the outgoing u quark into a Λ hyperon. In fact, the z distribution of Λ in the current fragmentation region is a measure of the $D^{\Lambda}_{u}(z)$ fragmentation function (normalized to unity in Fig. 15). The z distribution of $\bar{\Lambda}$ hyperons is sensitive to the $D^{\bar{\Lambda}}_{\bar{d}}(z)$ fragmentation function with a possible contribution from the $D^{\bar{\Lambda}}_{u}(z)$ process. One can see that it is harder than the one measured in the target fragmentation region.

4.3. Discussion

There are different mechanisms responsible for K^0_s, Λ and $\bar{\Lambda}$ production in the neutrino CC DIS process which are expected to give different x_F and z distributions for these particles.

- The x_F distribution of K^0_s mesons produced promptly in the $W^+ d \to u$ process that requires at least two quark–antiquark pairs to be created ($d\bar{d}$ and $s\bar{s}$) is expected to be central. A contribution from heavier strange particle decays (mainly from $K^{\star +}$) produced from the fragmentation of the outgoing u quark can result in a forward x_F distribution for K^0_s mesons. Also K^0_s mesons from a fragmentation of the outgoing (anti)quark in $W^+ d \to c \to s$ and $W^+ \bar{u} \to \bar{d}$ processes are expected to be produced in the forward x_F region and to carry a larger fraction of the jet energy.
- Λ hyperons can be produced from the fragmentation of the nucleon di-quark remnant promptly and via the decay of heavier strange baryons at $x_F < 0$. Λ hyperons can be produced also at $x_F > 0$ from the outgoing u quark fragmentation.
- The production of $\bar{\Lambda}$ hyperons in neutrino scattering from a valence quark requires three quark–antiquark pairs to be created ($u\bar{u}$, $d\bar{d}$ and $s\bar{s}$) and is expected to populate the central region of the x_F distribution. There could also be a contribution from the outgoing antiquark fragmentation into a $\bar{\Lambda}$ hyperon (in the $W^+ \bar{u} \to \bar{d} \to \bar{\Lambda}$ process) which can produce these baryons in the forward x_F region.

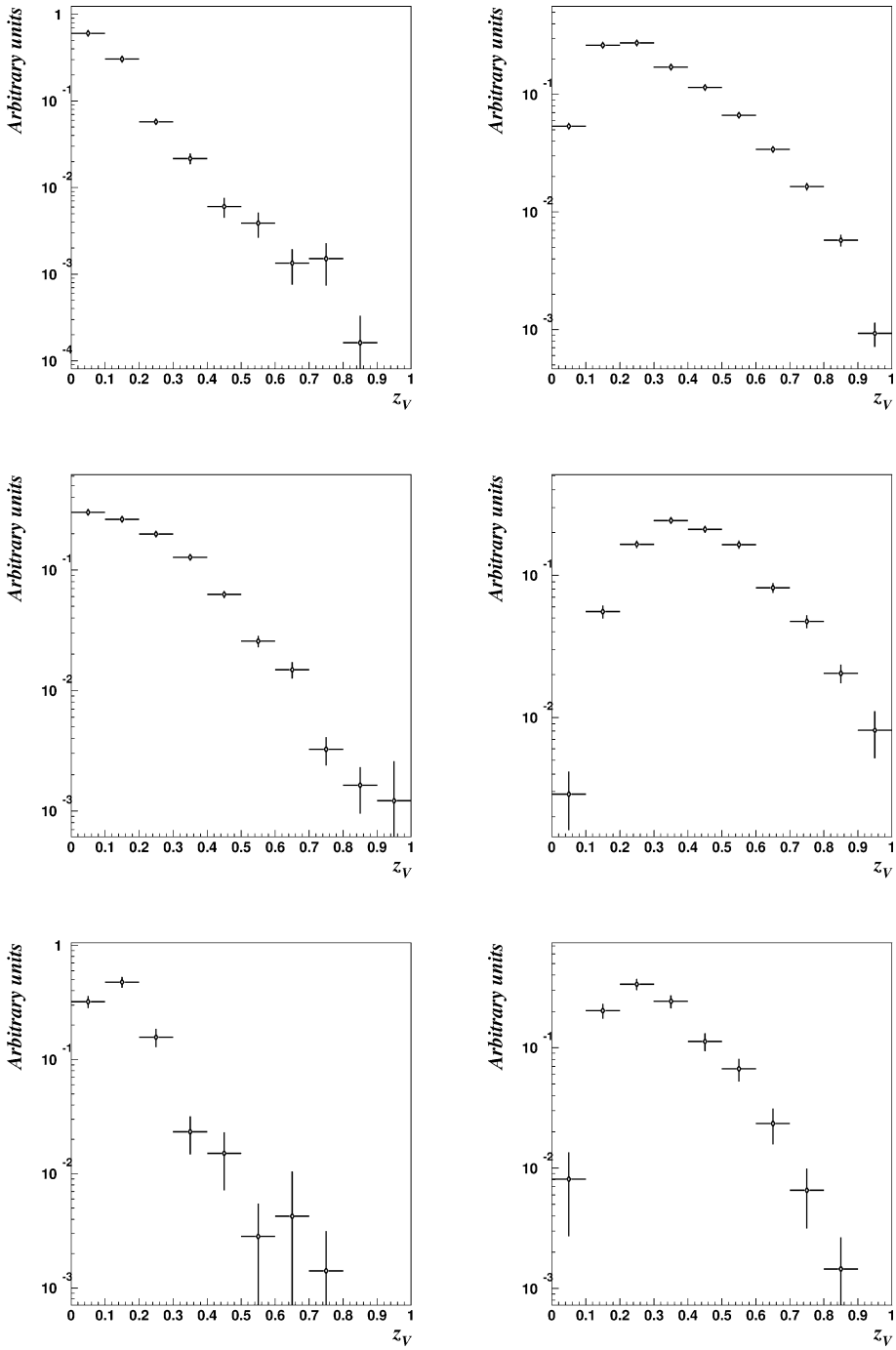

Fig. 15. Efficiency corrected z distributions for $x_F < 0$ (left) and for $x_F > 0$ (right) for K^0_S (top), Λ (center) and $\bar{\Lambda}$ (bottom).

4.4. p_T^2 distributions

The efficiency corrected p_T^2 distributions of K_s^0, Λ and $\bar{\Lambda}$ in the data are presented in Figs. 16–18. They show an exponential behaviour of the form $C \exp(-B \cdot p_T^2)$ in the region $p_T^2 \lesssim 0.5$ (GeV$^2/c^2$) and a deviation from this dependence at higher p_T^2. We measured the slope parameter B in the region $0 < p_T^2 < 0.5$ GeV$^2/c^2$ for each V^0 category in three kinematic regions: all x_F, $x_F < 0$ and $x_F > 0$. The results are listed in Table 10. The values of the slope parameter found in different x_F regions are similar, except for $\bar{\Lambda}$ hyperons.

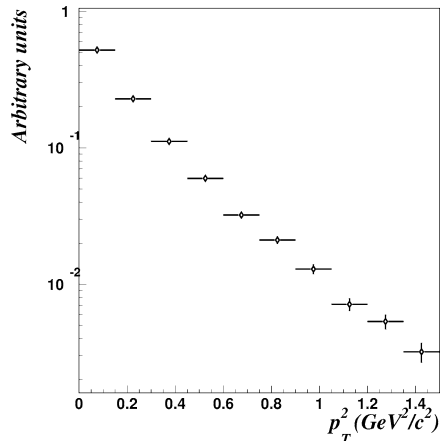

Fig. 16. Efficiency corrected p_T^2 distribution for K_s^0.

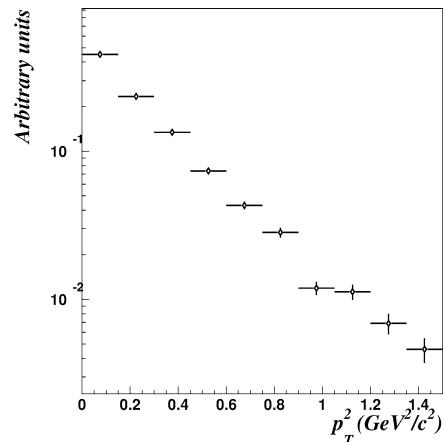

Fig. 17. Efficiency corrected p_T^2 distribution for Λ.

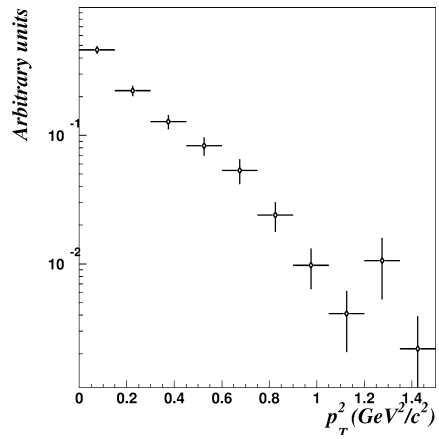

Fig. 18. Efficiency corrected p_T^2 distribution for $\bar{\Lambda}$.

Table 10
The slope parameter B $(\mathrm{GeV}/c)^{-2}$ of the p_T^2 distribution for K_s^0, Λ, $\bar{\Lambda}$ measured separately for the full sample and for $x_F < 0$ and $x_F > 0$ regions in both MC and data

V^0	MC			DATA		
	Full sample	$x_F < 0$	$x_F > 0$	Full sample	$x_F < 0$	$x_F > 0$
K_s^0	5.72 ± 0.03	5.61 ± 0.04	5.79 ± 0.03	5.21 ± 0.10	5.40 ± 0.21	5.15 ± 0.11
Λ	4.35 ± 0.03	4.30 ± 0.03	4.58 ± 0.06	4.12 ± 0.13	4.18 ± 0.15	4.07 ± 0.27
$\bar{\Lambda}$	3.89 ± 0.10	4.10 ± 0.13	3.70 ± 0.14	4.42 ± 0.47	6.59 ± 0.74	3.30 ± 0.64

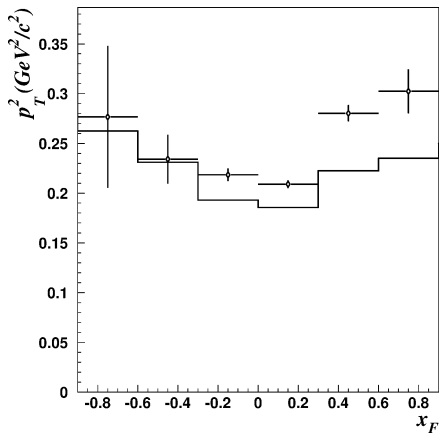

Fig. 19. Efficiency corrected $\langle p_T^2 \rangle$ versus x_F distribution for K_s^0 in data (points with error bars) and MC (histogram).

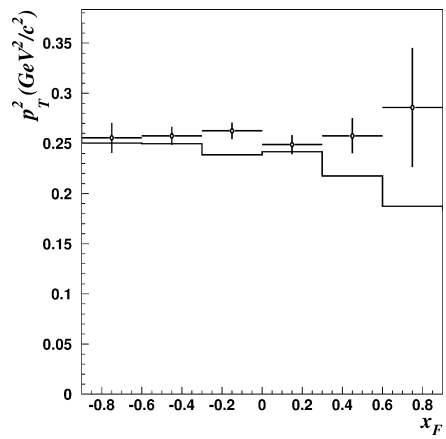

Fig. 20. Efficiency corrected $\langle p_T^2 \rangle$ versus x_F distribution for Λ in data (points with error bars) and MC (histogram).

4.5. $\langle p_T^2 \rangle$ versus x_F distributions

We have also studied the dependence of the average $\langle p_T^2 \rangle$ on x_F for K_s^0, Λ and $\bar{\Lambda}$ (see Figs. 19–21). For the first time in a neutrino experiment the good quality of event reconstruction combined with the large statistics of the data collected allows the study of these distributions for neutral strange particles.[3] The observed discrepancy between the data and simulated events in the region $x_F \gtrsim 0.3$ could be attributed to the absence of QCD effects in our Monte Carlo simulation program: the so-called soft-gluon effect could change the leading particle ($x_F \to 1$) behaviour inside the hadronic jet since the forward scattered quark is strongly accelerated and is therefore expected to radiate gluons, thus broadening the forward p_T^2 distribution. It has also been verified that there is no accumulation of misidentified V^0 in the region where the disagreement between the MC simulation and the data is observed.

[3] Similar distributions obtained for charged particles in bubble chamber neutrino experiments [47] have been used to tune Monte Carlo simulation programs.

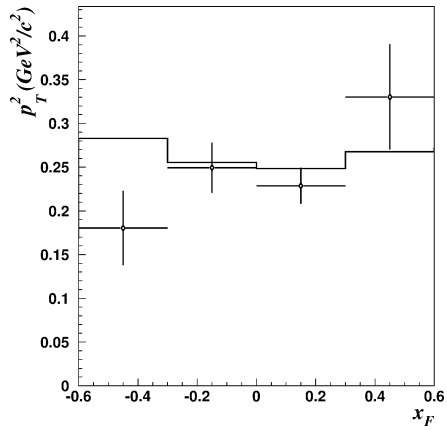

Fig. 21. Efficiency corrected $\langle p_T^2 \rangle$ versus x_F distribution for $\bar{\Lambda}$ in data (points with error bars) and MC (histogram).

5. Strange resonances and heavier hyperons

Apart from many good physics reasons a study of the production of resonances and heavy hyperons is also of great importance for tuning the LUND model parameters and for the theoretical interpretation of the Λ and $\bar{\Lambda}$ polarization measurements reported in our previous articles [27,28]. This is essential because Λ hyperons originating from the decays $\Sigma^\star \to \Lambda\pi$, $\Sigma^0 \to \Lambda\gamma$ and $\Xi \to \Lambda\pi$ inherit a polarization from the parent particles and this polarization is different from that of a directly produced Λ. Information about Σ^0, Ξ, $\Sigma^\star$, $\Xi^\star$ and $K^\star$ yields can be obtained from an analysis of their decays into channels containing identified neutral strange particles [39,48].

Previous bubble chamber experiments with (anti)neutrino beams suffered from a lack of statistics. For example, the BEBC WA21 Collaboration [24] reported the observation of 149 ± 29 $K^{\star+}$, 42 ± 19 $K^{\star-}$, 134 ± 19 $\Sigma^{\star+}$ and less than 10 $\Sigma^{\star-}$ in $\nu_\mu p$ CC interactions, while the Fermilab 15 ft bubble chamber E380 Collaboration [19] found 94 ± 25 Σ^0 and 4 Ξ^- in ν_μNe CC events.

5.1. A procedure for signal extraction

Our aim was to extract the fraction of neutral strange particles which are decay products of resonances and heavier hyperons from the corresponding invariant mass distributions. To construct such distributions we combine the neutral strange particle with all possible charged tracks (of appropriate sign) emerging from the primary vertex except those identified as muons or electrons. We have also studied the $(\Lambda\ \gamma)$ combinations, where photons are identified as conversions in the detector fiducial volume via our V^0 identification procedure. The resulting distributions are fitted by a function describing both the combinatorial background and the resonance signal.

The combinatorial background (BG) can be approximated by any function of the form:

$$\mathrm{BG} = P_n(m - M_{\mathrm{th}}) \cdot \mathrm{Tail}(m), \tag{2}$$

where $P_n(m - M_{\text{th}})$ is a polynomial of order n vanishing at $m = M_{\text{th}}$, $M_{\text{th}} = M_{V^0} + m_\pi$, and Tail$(m)$ is any function vanishing at $m \to \infty$ faster than P_n increases.

We have chosen the following BG parametrization:

$$\text{BG} = a_1 \Delta^{a_2} e^{-(a_3\Delta + a_4\Delta^2)}, \tag{3}$$

where $\Delta = m - M_{\text{th}}$.

For a resonance signal the standard relativistic Breit–Wigner (BW) function [49] is used:

$$\text{BW}(m) = \frac{\Gamma}{(m^2 - M_0^2)^2 + M_0^2\Gamma^2}\left(\frac{m}{q}\right), \quad \text{with } \Gamma = \Gamma_0\left(\frac{q}{q_0}\right)\frac{M_0}{m}, \tag{4}$$

where M_0, Γ_0 are the resonance mass and width, respectively, and q is the momentum of the decay product in the resonance rest frame (q_0 corresponds to M_0).

Finally, we have fitted the invariant mass distributions by:

$$\frac{dN}{dm} = \text{BG}(\Delta) + a_5\text{BW}'(m), \tag{5}$$

for all combinations except $(\Lambda\ \pi^-)$, where two peaks due to $\Sigma^{*-} \to \Lambda\pi^-$ and $\Xi^- \to \Lambda\pi^-$ decays are expected. Here $\text{BW}'(m)$ is the Breit–Wigner function of Eq. (4) normalized to unity. Such a fit is valid in all cases when the experimental mass resolution is small compared with the natural width of the resonance.

Similarly, for the $(\Lambda\ \pi^-)$ case we have used

$$\frac{dN}{dm} = \text{BG}(\Delta) + a_5\text{BW}'_{\Sigma^{*-}}(m) + a_6\text{BW}'_{\Xi^-}(m), \tag{6}$$

where the invariant mass resolution is used for the width Γ_0 in the Breit–Wigner function corresponding to the Ξ^- decay. In the above formulae a_1 to a_6 are parameters of the fit.

In such an approach using the HESSE and MINOS procedures of MINUIT [50], the parameter $a_5(a_6)$ gives the number of signal events with the corresponding error which takes into account possible correlations between different parameters.

As a consistency check we have also tried an alternative approach which was to fit the invariant mass distributions with:

$$\frac{dN}{dm} = \big(1 + a_5\text{BW}(m)\big)\text{BG}(\Delta), \tag{7}$$

and, similarly, with

$$\frac{dN}{dm} = \big(1 + a_5\text{BW}_{\Sigma^{*-}}(m) + a_6\text{BW}_{\Xi^-}(m)\big)\text{BG}(\Delta), \tag{8}$$

and extracted the corresponding number of signal events.

The results obtained using these two approaches were found to be similar. In what follows we present our results using the first method.

5.2. Results

The yields of resonances and heavy hyperons have been studied in different kinematic regions and for neutrino interactions on different target nucleons.

In NOMAD it is to some extent possible to separate neutrino interactions on the neutrons and protons by imposing a cut on the sum of charges ($Q_{\rm tot}$) of all the outgoing tracks at the primary neutrino interaction vertex.

We select νp events requiring $Q_{\rm tot} \geqslant 1$. According to the MC simulation, in this proton-like sample 76% of the events are true νp interactions. The νn events are selected by the requirement $Q_{\rm tot} \leqslant 0$. The purity of the corresponding neutron-like sample is about 85%.

Since the hadron production mechanisms in the target and in the current fragmentation regions are expected to be different, it is important to study separately the yields of resonances and heavy hyperons at $x_F < 0$ and $x_F > 0$. Such a study is also necessary for a correct theoretical interpretation of the Λ ($\bar{\Lambda}$) polarization measurements reported in our previous papers [27,28].

In the following we denote as MC(pred.) the true number of heavy strange particles reconstructed in the MC, and MC(meas.) the number of heavy strange particles extracted from the MC sample using our fitting procedure. Both quantities are normalized to the number of ν_μ CC events in the data.

Note that MC(pred.) and MC(meas.) can be slightly different due to limitations of the signal extraction procedure described in Section 5.1. The threshold and smearing effects in the invariant mass distributions are at the origin of this discrepancy. The ratio MC(pred.)/MC(meas.) will therefore be used to correct the yields of heavy strange particles extracted from the data (see Section 5.3).

The following resonances and heavier hyperons have been studied in the present analysis.

5.2.1. $K^{\star\pm}$

The fitted ($K^0_s\ \pi^\pm$) invariant mass distributions are shown in Fig. 22 for both MC and data samples. Detailed information on the number of extracted $K^{\star\pm}$ events and the $K^{\star\pm}/K^0_s$ ratio is given in Tables 11 and 12. For the $K^{\star\pm}$ mass and width we have used 891.66 MeV and 50.8 MeV, respectively. The q_0 value is 291 MeV/c [40].

Table 11
$K^{\star+} \to K^0_s\pi^+$ summary

$N(K^{\star+})$	Full sample	K^0_s fragmentation region		Type of target nucleon	
		$x_F < 0$	$x_F > 0$	νp	νn
DATA	2036 ± 121	315 ± 56	1731 ± 108	1006 ± 87	1032 ± 84
MC(meas.)	5373 ± 104	726 ± 47	4744 ± 93	1963 ± 67	3516 ± 80
MC(pred.)	5953	886	5067	2206	3748
$N(K^{\star+})/N(K^0_s)$			Uncorrected		
DATA (%)	13.5 ± 0.8	9.7 ± 1.7	14.6 ± 0.9	15.7 ± 1.4	11.9 ± 1.0
MC (%)	27.3 ± 0.5	14.5 ± 0.9	31.6 ± 0.6	29.0 ± 1.0	26.5 ± 0.6

Table 12
$K^{\star-} \to K^0_S \pi^-$ summary

$N(K^{\star-})$	Full sample	K^0_S fragmentation region		Type of target nucleon	
		$x_F < 0$	$x_F > 0$	νp	νn
DATA	1146 ± 89	288 ± 444	865 ± 78	377 ± 52	775 ± 73
MC(meas.)	2304 ± 74	639 ± 38	1664 ± 63	729 ± 39	1576 ± 63
MC(pred.)	2467	723	1743	734	1733
$N(K^{\star-})/N(K^0_S)$			Uncorrected		
DATA (%)	7.6 ± 0.6	8.9 ± 1.3	7.3 ± 0.7	5.9 ± 0.8	8.9 ± 0.8
MC (%)	11.5 ± 0.4	12.7 ± 0.8	11.1 ± 0.4	10.8 ± 0.6	11.9 ± 0.5

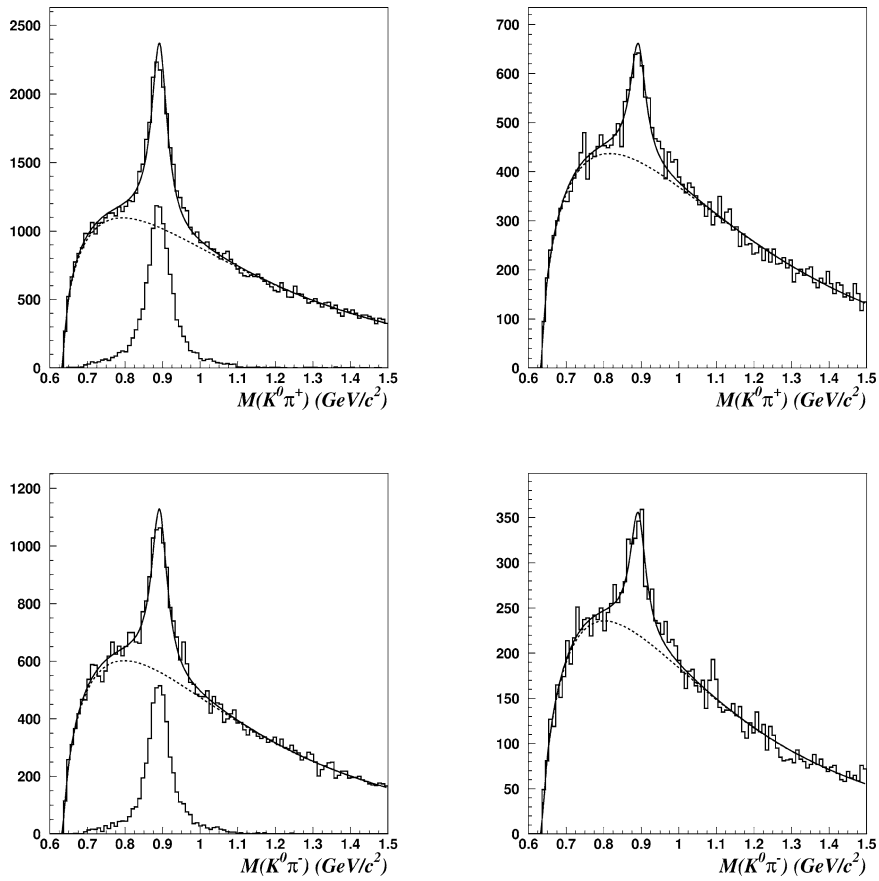

Fig. 22. $K^0_S \pi^+$ (top) and $K^0_S \pi^-$ (bottom) invariant mass distributions for both MC (left) and data (right). The solid lines are the results of the fit, while the dotted lines describe the background term. In the MC plots the additional histograms refer to the reconstructed true heavy strange particles.

It is interesting to note a more abundant $K^{\star+}$ than $K^{\star-}$ production in ν_μ CC DIS. This can be explained by the fact that the outgoing u quark can fragment directly into a $K^{\star+}$, while both $\bar{u}$ and s quarks needed to produce a $K^{\star-}$ meson have to be created in the fragmentation process.

One can see that there is a significant difference between $K^{\star\pm}$ yields in the default MC simulation and the NOMAD data (about a factor of 2).

5.2.2. $\Sigma^{\star\pm}$

For the $\Sigma^{\star\pm}$ mass and width we have taken the values from [40]: $m(\Sigma^{\star+}) = 1382.8$ MeV, $\Gamma(\Sigma^{\star+}) = 35.8$ MeV, $m(\Sigma^{\star-}) = 1387.2$ MeV, $\Gamma(\Sigma^{\star-}) = 39.4$ MeV. The q_0 value is 208 MeV/c.

The fitted invariant mass distributions for $(\Lambda\pi^{\pm})$ combinations in both MC and data samples are shown in Fig. 23. Detailed information on the number of extracted $\Sigma^{\star\pm}$ events

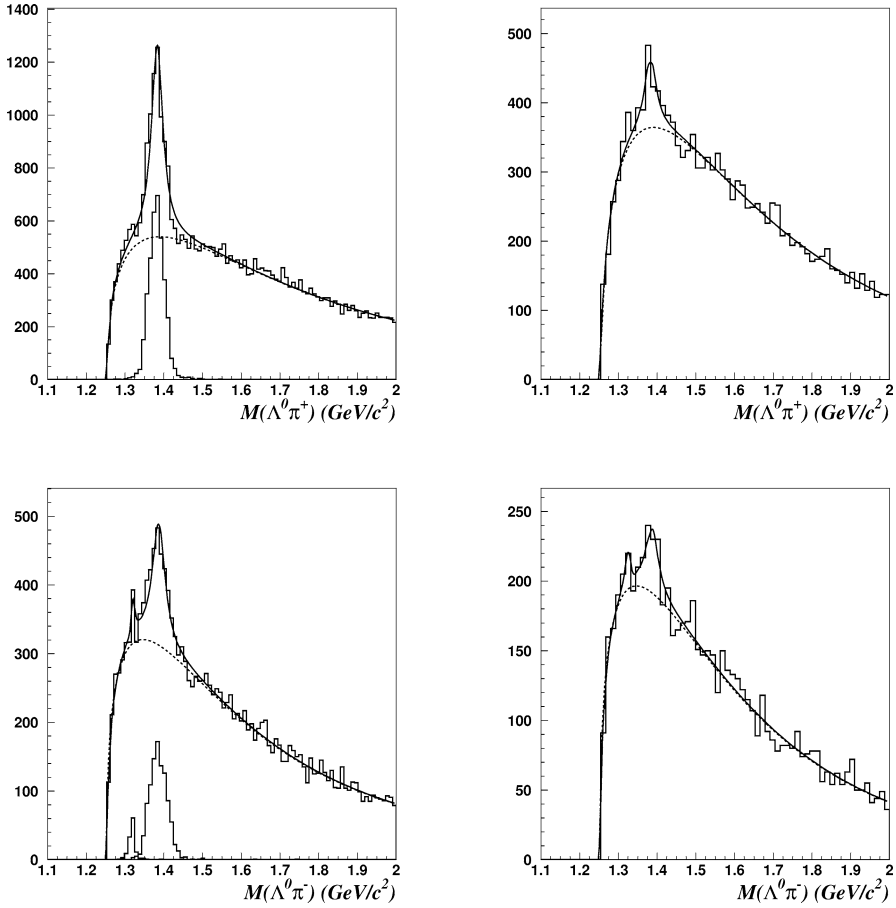

Fig. 23. $\Lambda\pi^+$ (top) and $\Lambda\pi^-$ (bottom) invariant mass distributions for both MC (left) and data (right). The solid lines are the results of the fit, while the dotted lines describe the background term. In the MC plots the additional histograms refer to the reconstructed true heavy strange particles.

Table 13
$\Sigma^{\star+} \to \Lambda\pi^+$ summary

$N(\Sigma^{\star+})$	Full sample	Λ fragmentation region		Type of target nucleon	
		$x_F < 0$	$x_F > 0$	vp	vn
DATA	416 ± 80	358 ± 65	63 ± 47	297 ± 61	120 ± 51
MC(meas.)	2070 ± 68	1427 ± 57	649 ± 37	1321 ± 49	754 ± 46
MC(pred.)	1783	1254	529	1150	634
$N(\Sigma^{\star+})/N(\Lambda)$			Uncorrected		
DATA (%)	5.2 ± 1.0	6.4 ± 1.2	2.5 ± 1.9	8.6 ± 1.8	2.6 ± 1.1
MC (%)	17.0 ± 0.6	15.9 ± 0.6	20.6 ± 1.2	32.6 ± 1.2	9.3 ± 0.6

Table 14
$\Sigma^{\star-} \to \Lambda\pi^-$ summary

$N(\Sigma^{\star-})$	Full sample	Λ fragmentation region		Type of target nucleon	
		$x_F < 0$	$x_F > 0$	vp	vn
DATA	206 ± 63	121 ± 51	93 ± 37	100 ± 35	111 ± 52
MC(meas.)	551 ± 48	410 ± 42	145 ± 25	18 ± 22	528 ± 43
MC(pred.)	489	362	126	33	456
$N(\Sigma^{\star-})/N(\Lambda)$			Uncorrected		
DATA (%)	2.6 ± 0.8	2.2 ± 0.9	3.7 ± 1.5	2.9 ± 1.0	2.4 ± 1.1
MC (%)	4.5 ± 0.4	4.6 ± 0.5	4.6 ± 0.8	0.4 ± 0.5	6.5 ± 0.5

and the $\Sigma^{\star\pm}/\Lambda$ ratio is given in Tables 13 and 14.

A striking difference between the $\Sigma^{\star\pm}$ yields in the default MC simulation and in the NOMAD data (a factor of about 3 or even larger) is observed.

5.2.3. Ξ^-

For the Ξ^- mass we have used 1321.32 MeV [40], for the width the experimental resolution of 10 MeV has been taken. The q_0 value is 139 MeV/c.

The bottom plots in Fig. 23 show evidence for $\Xi^- \to \Lambda\pi^-$ decays. Detailed information on the number of extracted Ξ^- events and the Ξ^-/Λ ratio is given in Table 15.

5.2.4. Σ^0

For the Σ^0 mass we have taken the value from [40]: $m(\Sigma^0) = 1192.6$ MeV, while for the width the experimental resolution of 9 MeV has been used. The q_0 value is 74 MeV/c. The Σ^0 peak has been fitted by a Gaussian function.

Table 15
$\Xi^- \to \Lambda\pi^-$ summary

$N(\Xi^-)$	Full sample	Λ fragmentation region		Type of target nucleon	
		$x_F < 0$	$x_F > 0$	νp	νn
DATA	42 ± 30	21 ± 24	18 ± 17	54 ± 18	-11 ± 24
MC(meas.)	43 ± 18	33 ± 15	13 ± 9	9 ± 8	36 ± 16
MC(pred.)	60	47	15	14	47
$N(\Xi^-)/N(\Lambda)$			Uncorrected		
DATA (%)	0.5 ± 0.4	0.4 ± 0.4	0.7 ± 0.7	1.6 ± 0.5	-0.2 ± 0.5
MC (%)	0.4 ± 0.2	0.4 ± 0.2	0.4 ± 0.3	0.2 ± 0.2	0.4 ± 0.2

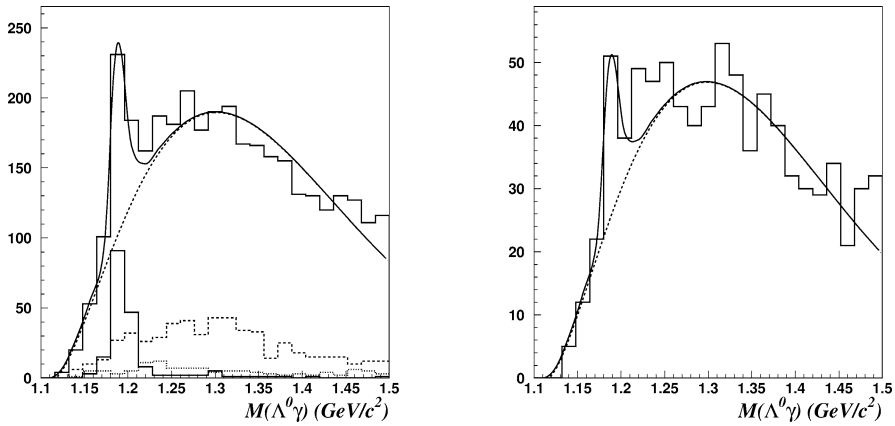

Fig. 24. $\Lambda\gamma$ invariant mass distributions for both MC (left) and data (right). The MC plot shows the expected signal peak and background contributions from $\Xi^0 \to \Lambda\pi^0$ and $\Sigma^{\star 0} \to \Lambda\pi^0$ decays with only one reconstructed photon.

Fig. 24 shows the fitted invariant mass distributions for $(\Lambda\ \gamma)$ combinations in both Monte Carlo and data samples. The corresponding photons have been reconstructed as conversions in the DC fiducial volume and identified by our V^0 identification procedure. The quality of the photon reconstruction is illustrated by the $(\gamma\gamma)$ invariant mass distributions shown in Fig. 25 for both MC and data: a peak corresponding to the π^0 signal is evident.

A summary of the number of extracted Σ^0 events and the Σ^0/Λ ratio is given in Table 16.

5.3. Yields of strange resonances and heavy hyperons

The integral yields of strange resonances and heavy hyperons produced in ν_μ CC are computed multiplying the results of the fits by the ratio MC(pred.)/MC(meas.).

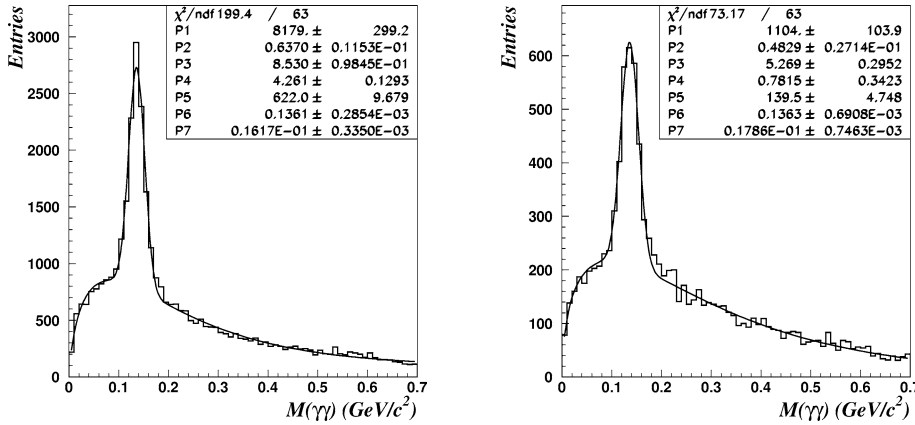

Fig. 25. $\gamma\gamma$ invariant mass distributions for MC (left) and data (right). Both photons have been reconstructed as conversions in the DC fiducial volume and identified by our V^0 identification procedure. A clear peak corresponding to the π^0 signal is visible in both distributions. The parameters P_6 and P_7 show the mass and the width of the Gaussian function after the fit.

Table 16
$\Sigma^0 \to \Lambda\gamma$ summary

$N(\Sigma^0)$	Full sample	Λ fragmentation region		Type of target nucleon	
		$x_F < 0$	$x_F > 0$	νp	νn
DATA	29 ± 10	17 ± 9	16 ± 7	16 ± 7	13 ± 7
MC(meas.)	82 ± 12	50 ± 9	37 ± 8	19 ± 7	61 ± 10
MC(pred.)	80	57	22	22	57
$N(\Sigma^0)/N(\Lambda)$			Uncorrected		
DATA (%)	0.4 ± 0.1	0.3 ± 0.2	0.7 ± 0.3	0.5 ± 0.2	0.3 ± 0.2
MC (%)	0.7 ± 0.1	0.6 ± 0.1	1.2 ± 0.3	0.5 ± 0.2	0.8 ± 0.1

Table 17
Corrected fractions (in %) of observed K^0_s and Λ decays that originate from the decays of strange resonances and heavy hyperons in the NOMAD data compared to the default MC predictions

	$K^{\star+} \to K^0_s\pi^+$	$K^{\star-} \to K^0_s\pi^-$	$\Sigma^{\star+} \to \Lambda\pi^+$	$\Sigma^{\star-} \to \Lambda\pi^-$	$\Sigma^0 \to \Lambda\gamma$	$\Xi^- \to \Lambda\pi^-$
DATA	15.5 ± 0.9	8.7 ± 0.7	5.8 ± 1.1	2.6 ± 0.8	7.3 ± 2.4	1.9 ± 1.7
MC	31.4	13.1	16.6	3.9	12.7	1.5

The results are presented in Table 17 as fractions of V^0 produced by heavy strange particles and resonances.

5.4. Discussion

The results of our study confirm discrepancies reported earlier [14] in the description of the strange resonances and heavy hyperons production in neutrino interactions by the LUND model with default parameters [30,31]. These results could be potentially used to tune the MC parameters responsible for the fragmentation into strange particles. Moreover, an additional analysis of events with multiple production of neutral strange particles could be very useful in this respect. Such an analysis is currently in progress.

6. Conclusion

We have reported the results of a study of strange particle production in ν_μ CC interactions using the data from the NOMAD experiment. Our analysis is based on a sample of ν_μ CC events containing 15074 identified K^0_S, 8087 identified Λ and 649 identified $\bar{\Lambda}$ decays. This V^0 sample represents at least a factor of 5 increase in statistics compared to previous (anti)neutrino experiments performed with bubble chambers. Yields of neutral strange particles (K^0_S, Λ, $\bar{\Lambda}$) have been measured in this analysis as a function of kinematic variables. For $\bar{\Lambda}$ production such measurements are performed for the first time in a neutrino experiment. The decays of resonances and heavy hyperons with identified K^0_S and Λ in the final state have been analyzed. Clear signals corresponding to $K^{\star\pm}$, $\Sigma^{\star\pm}$, Ξ^- and Σ^0 have been observed. This study is potentially interesting for the tuning of Monte Carlo simulation programs and is also of special importance for a quantitative theoretical interpretation of the Λ and $\bar{\Lambda}$ polarization measurements reported earlier [27,28].

Acknowledgements

We gratefully acknowledge the CERN SPS accelerator and beam-line staff for the magnificent performance of the neutrino beam. We also thank the technical and secretarial staff of the collaborating institutes. The experiment was supported by the following funding agencies: Australian Research Council (ARC) and Department of Industry, Science, and Resources (DISR), Australia; Institut National de Physique Nucléaire et Physique des Particules (IN2P3), Commissariat à l'Energie Atomique (CEA), France; Bundesministerium für Bildung und Forschung (BMBF, contract 05 6DO52), Germany; Istituto Nazionale di Fisica Nucleare (INFN), Italy; Joint Institute for Nuclear Research and Institute for Nuclear Research of the Russian Academy of Sciences, Russia; Fonds National Suisse de la Recherche Scientifique, Switzerland; Department of Energy, National Science Foundation (grant PHY-9526278), the Sloan and the Cottrell Foundations, USA.

References

[1] S.J. Barish et al., Phys. Rev. Lett. 33 (1974) 1446.
[2] H. Deden et al., Phys. Lett. B 58 (1975) 361.
[3] J.P. Berge et al., E45 Collaboration, Phys. Rev. Lett. 36 (1976) 127.
[4] H. Deden et al., Phys. Lett. B 67 (1977) 474.
[5] J.P. Berge et al., E45 Collaboration, Phys. Rev. D 18 (1978) 1359.
[6] O. Erriquez et al., Nucl. Phys. B 140 (1978) 123.
[7] V.V. Ammosov et al., Nucl. Phys. B 162 (1980) 205.
[8] N.J. Baker et al., E427 Collaboration, Phys. Rev. D 24 (1981) 2779.
[9] V.V. Ammosov et al., Nucl. Phys. B 177 (1981) 365.
[10] R. Brock et al., E31 Collaboration, Phys. Rev. D 25 (1982) 1753.
[11] H. Grässler et al., Nucl. Phys. B 194 (1982) 1.
[12] P. Bosetti et al., WA47 Collaboration, Nucl. Phys. B 209 (1982) 29.
[13] D. Son et al., Phys. Rev. Lett. 49 (1982) 1128;
D. Son et al., Phys. Rev. Lett. 49 (1982) 1800, Erratum.
[14] D. Allasia et al., WA25 Collaboration, Nucl. Phys. B 224 (1983) 1.
[15] C.C. Chang et al., Phys. Rev. D 27 (1983) 2776.
[16] D. Son et al., Phys. Rev. D 28 (1983) 2129.
[17] D. Allasia et al., WA25 Collaboration, Phys. Lett. B 154 (1985) 231.
[18] G.T. Jones et al., WA21 Collaboration, Z. Phys. C 28 (1985) 23.
[19] N.J. Baker et al., E380 Collaboration, Phys. Rev. D 34 (1986) 1251.
[20] W.A. Mann et al., Phys. Rev. D 34 (1986) 2545.
[21] V.V. Ammosov et al., SKAT Collaboration, Z. Phys. C 30 (1986) 183.
[22] V.V. Ammosov et al., Z. Phys. C 36 (1987) 377.
[23] S. Willocq et al., WA59 Collaboration, Z. Phys. C 53 (1992) 207.
[24] G.T. Jones et al., WA21 Collaboration, Z. Phys. C 57 (1993) 197.
[25] D. DeProspo et al., E632 Collaboration, Phys. Rev. D 50 (1994) 6691.
[26] J. Altegoer et al., NOMAD Collaboration, Nucl. Instrum. Methods A 404 (1998) 96.
[27] P. Astier et al., NOMAD Collaboration, Nucl. Phys. B 588 (2000) 3.
[28] P. Astier et al., NOMAD Collaboration, Nucl. Phys. B 605 (2001) 3.
[29] J. Altegoer et al., NOMAD Collaboration, Phys. Lett. B 431 (1998) 219;
P. Astier et al., NOMAD Collaboration, Phys. Lett. B 453 (1999) 169;
P. Astier et al., NOMAD Collaboration, Phys. Lett. B 483 (2000) 387;
P. Astier et al., NOMAD Collaboration, Nucl. Phys. B 611 (2001) 3.
[30] G. Ingelman, LEPTO version 6.1, The Lund Monte Carlo for Deep Inelastic Lepton–Nucleon Scattering, TSL-ISV-92-0065, 1992;
G. Ingelman, A. Edin, J. Rathsman, LEPTO version 6.5, Comput. Phys. Commun. 101 (1997) 108, hep-ph/9605286.
[31] T. Sjöstrand, PYTHIA 5.7 and JETSET 7.4: physics and manual, LU-TP-95-20 (1995), hep-ph/9508391;
T. Sjöstrand, Comput. Phys. Commun. 39 (1986) 347;
T. Sjöstrand, Comput. Phys. Commun. 43 (1987) 367.
[32] GEANT: Detector Description and Simulation Tool, CERN Programming Library Long Writeup W 5013, GEANT version 3.21.
[33] M. Glück, E. Reya, A. Vogt, Z. Phys. C 53 (1992) 127.
[34] H. Plothow-Besch, Comput. Phys. Commun. 75 (1993) 396.
[35] P. Astier et al., NOMAD Collaboration, Prediction of neutrino fluxes in the NOMAD experiment, in preparation.
[36] M. Anfreville et al., The drift chambers of the NOMAD experiment, hep-ex/0104012, to be published in Nucl. Instrum. Methods.

[37] G. Bassompierre et al., Nucl. Instrum. Methods A 403 (1998) 363;
G. Bassompierre et al., Nucl. Instrum. Methods A 411 (1998) 63.
[38] D. Autiero et al., Nucl. Instrum. Methods A 373 (1996) 358;
D. Autiero et al., Nucl. Instrum. Methods A 387 (1997) 352;
D. Autiero et al., Nucl. Instrum. Methods A 411 (1998) 285.
[39] D.V. Naumov, Ph.D. Thesis, JINR, Dubna, Russia, 2001, in Russian.
[40] Review of Particle Properties, Eur. Phys. J. C 15 (2000).
[41] G.T. Jones et al., WA21 Collaboration, Z. Phys. C 27 (1985) 43.
[42] P.D. Acton et al., OPAL Collaboration, Z. Phys. C 56 (1992) 521.
[43] P. Abreu et al., DELPHI Collaboration, Z. Phys. C 65 (1995) 587.
[44] M.R. Adams et al., E665 Collaboration, Z. Phys. C 61 (1994) 539.
[45] M. Derrick et al., ZEUS Collaboration, Z. Phys. C 68 (1995) 29.
[46] S. Aid et al., H1 Collaboration, Nucl. Phys. B 480 (1996) 3.
[47] P.C. Bosetti et al., WA21 & WA47 Collaborations, Z. Phys. C 46 (1990) 377;
G.T. Jones et al., WA21 Collaboration, Z. Phys. C 25 (1984) 121.
[48] C. Lachaud, Ph.D. Thesis, Université Denis Diderot (Paris 7), May, 2000, in French.
[49] J.D. Jackson, Nuovo Cimento 34 (1964) 1644.
[50] MINUIT package, CERN Program Library Long Writeup D 506 (1994).